Chapter 1
Remote Sensing of Coastal Ecosystems and Environments

Victor V. Klemas

Abstract Advances in sensor design and data analysis techniques are making remote sensing systems suitable for monitoring coastal ecosystems and their changes. Hyperspectral imagers, LiDAR and radar systems are available for mapping coastal marshes, submerged aquatic vegetation, coral reefs, beach profiles, algal blooms, and concentrations of suspended particles and dissolved substances in coastal waters. Since coastal ecosystems have high spatial complexity and temporal variability, they benefit from new satellites, carrying sensors with fine spatial (0.4–4 m) or spectral (200 narrow bands) resolution. Imaging radars are sensitive to soil moisture and inundation and can detect hydrologic features beneath the vegetation canopy. Multi-sensor and multi-seasonal data fusion techniques are significantly improving coastal land cover mapping accuracy and efficiency. Using time-series of images enables scientists to study coastal ecosystems and to determine long- term trends and short- term changes.

1.1 Introduction

Coastal ecosystems, including marshes, mangroves, seagrasses and coral reefs, are highly productive and act as critical habitats for a wide variety of plants, fish, shellfish, and other wildlife. For instance, coastal wetlands provide flood protection, protection from storm and wave damage, water quality improvement through filtering of agricultural and industrial waste, and recharge of aquifers (Morris et al. 2002; Odum 1993). Since more than half of the U.S. population lives in the coastal zone, coastal ecosystems have been exposed to a wide range of stress-inducing alterations, including dredge and fill operations, hydrologic modifications,

V.V. Klemas (✉)
School of Marine Science and Policy, University of Delaware, Newark, DE 19716, USA
e-mail: klemas@udel.edu

C.W. Finkl and C. Makowski (eds.), *Remote Sensing and Modeling: Advances in Coastal and Marine Resources*, Coastal Research Library 9,
DOI 10.1007/978-3-319-06326-3_1,

pollutant run-off, eutrophication, impoundments and fragmentation by roads and ditches (Waycott et al. 2009). Furthermore, with events such as the hurricanes of 2004, 2005 and 2012 annual losses to coastal communities can total billions of dollars. Environmental impacts from coastal storms include beach erosion, wetland destruction, excessive nutrient loading, algal blooms, hypoxia and anoxia, fish kills, releases of pollutants, spread of pathogens, and bleaching of coral reefs.

Over the long term, coastal communities are also facing a rising sea level. The substantial sea level rise and more frequent storms predicted for the next 50–100 years will affect coastal towns and roads, coastal economic development, beach erosion control strategies, salinity of estuaries and aquifers, coastal drainage and sewage systems, and coastal wetlands and coral reefs (Gesch 2009; IPCC 2007; NOAA 1999). Coastal areas such as barrier islands, beaches, and wetlands are especially sensitive to sea-level changes. A major hurricane can devastate a wetland (Klemas 2009). Rising seas will intensify coastal flooding and increase the erosion of beaches, bluffs and wetlands, as well as threaten jetties, piers, seawalls, harbors, and waterfront property. Along barrier islands, the erosion of beachfront property by flooding water will be severe, leading to greater probability of overwash during storm surges (NOAA 1999).

Since coastal ecosystems have high spatial complexity and temporal variability, they require high spatial, spectral and temporal resolutions. Recent advances in sensor design and data analysis techniques are making remote sensing systems practical and cost-effective for monitoring natural and man-made changes impacting coastal ecosystems. High resolution multispectral and hyperspectral imagers, LiDAR and radar systems are available for monitoring changes in coastal marshes, submerged aquatic vegetation, coral reefs, beach profiles, algal blooms, and concentrations of suspended particles and dissolved substances in coastal waters. Some of the ecosystem health indicators that can be mapped with new high-resolution remote sensors include natural vegetation cover, wetland loss and fragmentation, wetland biomass change, percent of impervious watershed area, buffer degradation, changes in hydrology, water turbidity, chlorophyll concentration, eutrophication level, salinity, *etc*. (Lathrop et al. 2000; Martin 2004; Wang 2010).

With the rapid development of new remote sensors, data bases and image analysis techniques, potential users need guidance in choosing remote sensors and data analysis methods that are most appropriate for each specific coastal application (Yang 2009). The objective of this paper is to review those remote sensing techniques that are cost-effective and practical for shoreline delineation, wetland mapping and other coastal applications.

1.2 Wetland Mapping

For more than three decades remote sensing techniques have been used by researchers and government agencies to map and monitor wetlands (Dahl 2006; Tiner 1996). Traditionally, in addition to airborne sensors, the Landsat Thematic Mapper (TM) and the French SPOT satellite have been reliable data sources for

Fig. 1.1 The Moderate Resolution Imaging Spectroradiometer (MODIS) on NASA's Terra satellite captured this image on September 26, 2008, 13 days after Hurricane Ike came ashore. The *brown* areas in the image are the result of a massive storm surge that Ike pushed far inland over Texas and Louisiana causing a major marsh dieback (Color figure online) (Credits: NASA/GSFC)

wetland and land cover mapping (Klemas 2011). Their 30 m and 10–20 m respective spatial resolutions and spectral bands have proven cost-effective for mapping land cover and changes in large coastal watersheds (Harvey and Hill 2001; Houhoulis and Michener 2000; Jensen 2007; Lunetta and Balogh 1999). Landsat TM and ETM+ imagery have also been used to study water turbidity and depth in marshes as well as the seasonal dynamics of inundation, turbidity, and vegetation cover (Bustamante et al. 2009; Ward et al. 2012).

More recently other medium spatial resolution satellite sensors, such as MODIS on NASA's Terra and Aqua satellites, have been used to map wetlands and study their interaction with storm surges. This is illustrated in Fig. 1.1, which shows an image of the Texas coast captured by MODIS on NASA's Terra satellite 13 days after Hurricane Ike made landfall on September 13, 2008. The storm's surge covered hundreds of kilometers of the Gulf Coast because Ike was a large storm, with tropical-storm-strength winds stretching more than 400 km from the center of the storm. Most of the shoreline in this region is coastal wetland. One can clearly distinguish the red-brown areas in the image which are the result of the massive storm surge that Ike had pushed far inland over Texas and Louisiana, causing a major marsh dieback. The salty water burned the plants, leaving them wilted and brown. The brown line corresponds with the location and extent of the wetlands. North of the brown line, the vegetation gradually transitions to pale green farmland

and dark green natural vegetation untouched by the storm's surge. The powerful tug of water returning to the Gulf also stripped marsh vegetation and soil off the land. Therefore, some of the brown seen in the wetlands may be deposited sediment. Plumes of brown water are visible as sediment-laden water drains from rivers and the coast in general. The muddy water slowly diffuses, turning pale green, green, and finally blue as it blends with clearer Gulf water (NASA/GSFC 2010; Ramsey and Rangoonwala 2005).

Many coastal ecosystems are patchy and exhibit considerable variations in their extent, spatial complexity, and temporal variability (Dahl 2006). Protecting them requires the ability to monitor their biophysical features and controlling processes at high spatial and temporal resolutions, such as that provided by aircraft and high spatial resolution satellite sensors (Adam et al. 2010; Klemas 2011). More recently, the availability of high spatial and spectral resolution satellite data has significantly improved the capacity for mapping salt marshes and other coastal ecosystems (Jensen et al. 2007; Laba et al. 2008; Ozesmi and Bauer 2002; Wang et al. 2010). High resolution imagery (0.4–4 m) can now be obtained from satellites, such as IKONOS and QuickBird. Major plant species within a complex, heterogeneous tidal marsh have been classified using multitemporal high-resolution QuickBird images, field reflectance spectra and LiDAR height information. *Phragmites*, *Typha* spp. and *S. patens* were spectrally distinguishable at particular times of the year, likely due to differences in biomass and pigments and the rate at which change occurred throughout the growing season. For instance, classification accuracies for *Phragmites* were high due to the uniquely high near-infrared reflectance and height of this plant in the early fall (Ghioca-Robrecht et al. 2008; Gilmore et al. 2010).

High resolution imagery is more sensitive to within- class spectral variance, making separation of spectrally mixed land cover types more difficult than when using medium resolution imagery. Therefore, pixel-based techniques are sometimes replaced by object-based methods, which incorporate spatial neighborhood properties, by segmenting/partitioning the image into a series of closed objects which coincide with the actual spatial pattern, and then proceed to classify the image. "Region growing" is among the most commonly used segmentation methods. This procedure starts with the generation of seed points over the whole scene, followed by grouping neighboring pixels into an object under a specific homogeneity criterion. Thus the object keeps growing until its spectral closeness metric exceeds a predefined break-off value (Kelly and Tuxen 2009; Shan and Hussain 2010; Wang et al. 2004).

Small wetland sites are often mapped and studied using airborne sensors (Jensen 2007; Klemas 2011). Airborne georeferenced digital cameras, providing color and color infrared digital imagery are particularly suitable for accurate wetland mapping and interpreting satellite data. Most digital cameras are capable of recording reflected visible to near-infrared light. A filter is placed over the lens that transmits only selected portions of the wavelength spectrum. For a single camera operation, a filter is chosen that generates natural color (blue-green-red wavelengths) or color-infrared (green-red-near IR wavelengths) imagery. For multiple camera operation, filters that transmit narrower bands are chosen (Ellis and Dodd 2000).

Digital camera imagery can be integrated with GPS position information and used as layers in a GIS for a wide range of modeling applications (Lyon and McCarthy 1995). Small aircraft flown at low altitudes (*e.g.* 200–500 m) can also be used to guide field data collection (McCoy 2005). However, cost becomes excessive if the study site is larger than a few hundred square kilometers, and in that case, medium resolution multispectral sensors, such as Landsat TM (30 m) and SPOT (20 m), become more cost-effective (Klemas 2011).

1.3 Hyperspectral Remote Sensing of Wetlands

Airborne hyperspectral imagers, such as the Advanced Visible Infrared Imaging Spectrometer (AVIRIS) and the Compact Airborne Spectrographic Imager (CASI) have been used for mapping coastal wetlands and shallow water substrate (Fearns et al. 2011; Lesser and Mobley 2007; Li et al. 2005; Rosso et al. 2005; Ozesmi and Bauer 2002; Schmidt and Skidmore 2003; Thomson et al. 1998). Hyperspectral imagers may contain hundreds of narrow spectral bands located in the visible, near-infrared, mid-infrared, and sometimes thermal portions of the EM spectrum (Jensen et al. 2007).

The advantages and problems associated with hyperspectral mapping have been clearly demonstrated by Hirano et al. (2003) who used AVIRIS hyperspectral data to map vegetation for a portion of Everglades National Park in Florida. The AVIRIS provides 224 spectral bands from 0.4 to 2.45 μm, each with 0.01 μm bandwidth, 20 m spatial resolution, and a swath width of 10.5 km. Hirano et al. compared the geographic locations of spectrally pure pixels in the AVIRIS image with dominant vegetation polygons of the Everglades Vegetation Database and identified spectrally pure pixels as ten different vegetation classes, plus water and mud. An adequate number of pure pixels was identified to permit the selection of training samples used in the automated classification procedure. The spectral signatures from the training samples were then matched to the spectral signatures of each individual pixel. Image classification was undertaken using the ENVI spectral angle mapper (SAM) classifier in conjunction with the spectral library created for the Everglades study area. The SAM classifier examines the digital numbers (DNs) of all bands from each pixel in the AVIRIS data set to determine similarity between the angular direction of the spectral signature (*i.e.* color) of the image pixel and that of a specific class in the spectral library. A coincident or small spectral angle between the vector for the unknown pixel and that for a vegetation class training sample indicates that the image pixel likely belongs to that vegetation class. In the case of spectrally mixed pixels, the relative probability of membership (based on the spectral angle) to all vegetation classes is calculated. Mixed pixels are then assigned to the class of the greatest probability of membership (Hirano et al. 2003).

The hyperspectral data proved effective in discriminating spectral differences among major Everglades plants such as red, black and white mangrove communities and enabled the detection of exotic invasive species (Hirano et al. 2003). The overall classification accuracy for all vegetation pixels was 65.7 %, with different mangrove

tree species ranging from 73.5 to 95.7 % correct. Limited spatial resolution was a problem, resulting in too many mixed pixels. Another problem was the complexity of image-processing procedures that are required before the hyperspectral data can be used for automated classification of wetland vegetation. The tremendous volume of hyperspectral image data necessitated the use of specific software packages, large data storage, and extended processing time (Hirano et al. 2003). A detailed accuracy assessment of airborne hyperspectral data for mapping plant species in freshwater coastal wetlands has been performed by Lopez et al. (2004).

A number of advanced new techniques have been developed for mapping wetlands and even identifying wetland types and plant species (Schmidt et al. 2004; Jensen et al. 2007; Klemas 2011; Yang et al. 2009). For instance, using LiDAR, hyperspectral and radar imagery, and narrow-band vegetation indices, researchers have been able not only discriminate some wetland species, but also make progress on estimating biochemical and biophysical parameters of wetland vegetation, such as water content, biomass and leaf area index (Adam et al. 2010; Artigas and Yang 2006; Filippi and Jensen 2006; Gilmore et al. 2010; Ozesmi and Bauer 2002; Simard et al. 2010; Wang 2010). The integration of hyperspectral imagery and LiDAR-derived elevation has also significantly improved the accuracy of mapping salt marsh vegetation. The hyperspectral images help distinguish high marsh from other salt marsh communities due to its high reflectance in the near-infrared region of the spectrum, and the LiDAR data help separate invasive *Phragmites* from low marsh plants (Yang and Artigas 2010).

Hyperspectral imaging systems are now available not only for airborne applications, but also in space, such as the satellite-borne Hyperion system, which can detect fine differences in spectral reflectance, assisting in species discrimination on a global scale (Christian and Krishnayya 2009; Pengra et al. 2007). The Hyperion sensor provides imagery with 220 spectral bands at a spatial resolution of 30 m. Although there have been few studies using satellite-based hyperspectral remote sensing to detect and map coastal vegetation species, results so far have shown that discrimination between multiple species is possible (Blasco et al. 2005; Heumann 2011).

1.4 Wetland Applications of Synthetic Aperture Radar (SAR)

Imaging radars provide information that is fundamentally different from sensors that operate in the visible and infrared portions of the electromagnetic spectrum. This is primarily due to the much longer wavelengths used by SAR sensors and the fact that they send out and receive their own energy (*i.e.*, active sensors). One of the most common types of imaging radar is Synthetic Aperture Radar (SAR). SAR technology provides the increased spatial resolution that is necessary in regional wetland mapping and SAR data have been used extensively for this purpose (Lang and McCarty 2008; Novo et al. 2002).

When mapping and monitoring wetland ecosystems, imaging radars have some advantages over sensors that operate in the visible and infrared portions of the electromagnetic spectrum. Microwave energy is sensitive to variations in soil moisture and inundation, and is only partially attenuated by vegetation canopies, especially in areas of lower biomass (Baghdadi et al. 2001; Kasischke et al. 1997a, b; Lang and Kasischke 2008; Rosenqvist et al. 2007; Townsend 2000, 2002; Townsend and Walsh 1998) or when using data collected at longer wavelengths (Hess et al. 1990; Martinez and Le Toan 2007).

The sensitivity of microwave energy to water and its ability to penetrate vegetative canopies, make SAR ideal for the detection of hydrologic features below the vegetation (Kasischke et al. 1997a; Kasischke and Bourgeau-Chavez 1997; Phinn et al. 1999; Rao et al. 1999; Wilson and Rashid 2005). The presence of standing water interacts with the radar signal differently depending on the dominant vegetation type/structure (Hess et al. 1995) as well as the biomass and condition of vegetation (Costa and Telmer 2007; Töyrä et al. 2002). When exposed to open water without vegetation, specular reflection occurs and a dark signal (weak or no return) is observed (Dwivedi et al. 1999). The radar signal is often reduced in wetlands dominated by lower biomass herbaceous vegetation when a layer of water is present due largely to specular reflectance (Kasischke et al. 1997a). Conversely, the radar signal is often increased in forested wetlands when standing water is present due to the double-bounce effect (Harris and Digby-Arbus 1986; Dwivedi et al. 1999). This occurs in flooded forests when the radar pulse is reflected strongly by the water surface away from the sensor (specular reflectance) but is then redirected back towards the sensor by a second reflection from a nearby tree trunk. The use of small incidence angles (closer to nadir) enhances the ability to map hydrology beneath the forest canopy due to increased penetration of the canopy (Bourgeau-Chavez et al. 2001; Hess et al. 1990; Lang and McCarty 2008; Töyrä et al. 2001).

1.5 Wetland Change Detection

Many coastal wetlands, such as the tidal salt marshes along the Louisiana coast, are generally within fractions of a meter of sea level and will be lost, especially if the impact of sea level rise is amplified by coastal storms. Man-made modifications of wetland hydrology and extensive urban development will further limit the ability of wetlands to survive sea level rise. To identify long-term trends and short term variations, such as the impact of rising sea levels and storm surges on wetlands, one needs to analyze time-series of remotely sensed imagery. High temporal resolution, precise spectral bandwidths, and accurate georeferencing procedures are factors that contribute to the frequent use of satellite image data for change detection analysis (Baker et al. 2007; Coppin et al. 2004; Shalabi and Tateishi 2007). A good example is the study of the onset and progression of marsh dieback performed by Ramsey and Rangoonwala (2010).

The acquisition and analysis of time-series of multi-spectral imagery is a challenging task. The imagery must be acquired under similar environmental conditions (*e.g.* same time of year, sun angle, *etc.*) and in the same or similar spectral bands. There will be changes in both, time and spectral content. One way to approach this problem is to reduce the spectral information to a single index, reducing the multispectral imagery into one single field of the index for each time step. In this way the problem is simplified to the analysis of a time-series of a single variable, one for each pixel of the images.

The most common index used is the Normalized Difference Vegetation Index (NDVI), which is expressed as the difference between the red and near infrared (NIR) reflectances divided by their sum (Jensen 2007). These two spectral bands represent the most detectable spectral characteristic of green plants. This is because the red (and blue) radiation is absorbed by the chlorophyll in the surface layers of the plant (*Palisade parenchyma*) and the NIR is reflected from the inner leaf cell structure (*Spongy mesophyll*) as it penetrates several leaf layers in a canopy. Thus the NDVI can be related to plant biomass or stress, since the NIR reflectance depends on the abundance of plant tissue, whereas the red reflectance indicates the surface condition of the plant. It has been shown by researchers that time-series remote sensing data can be used effectively to identify long term trends and subtle changes of NDVI by means of Principal Component Analysis (Jensen 2007; Young and Wang 2001; Yuan et al. 1998).

The pre-processing of multi-date sensor imagery when absolute comparisons between different dates are to be carried out, is much more demanding than the single-date case. It requires a sequence of operations, including calibration to radiance or at-satellite reflectance, atmospheric correction, image registration, geometric correction, mosaicking, sub-setting, and masking out clouds and irrelevant features (Coppin et al. 2004; Lunetta and Elvidge 1998).

Detecting the actual changes between two registered and radiometrically corrected images from different dates can be accomplished by employing one of several techniques, including post-classification comparison (PCC), spectral image differencing (SID), and change vector analysis (CVA). In PCC change detection, two images from different dates are independently classified. The two classified maps are then compared on a pixel-by-pixel basis. One disadvantage is that every error in the individual date classification maps will also be present in the final change detection map (Jensen 1996; Lunetta and Elvidge 1998).

Spectral image differencing (SID) is the most widely applied change detection algorithm. SID techniques rely on the principle that land cover changes result in changes in the spectral signature of the affected land surface. SID techniques involve the transformation of two original images to a new single-band or multiband image in which the areas of spectral change are highlighted. This is accomplished by subtracting one date of raw or transformed (*e.g.* vegetation indices, albedo, *etc.*) imagery from a second date, which has been precisely registered to the image of the first date. Pixel difference values exceeding a selected threshold are considered as changed. This approach eliminates the need to identify land cover changes in areas where no significant spectral change has occurred between the two

dates of imagery (Coppin et al. 2004; Jensen 1996). A comparison of the SID and the PCC change detection algorithms is provided by Macleod and Congalton (1998). The SID and the PCC based change detection methods are often combined in a hybrid approach. For instance, SID can be used to identify areas of significant spectral change, and then PCC can be applied within areas where spectral change was detected in order to obtain class-to-class change information.

The changeable nature of wetland ecosystems sometimes requires a more dynamic change detection procedure. These ecosystems can exhibit a variety of vegetative or hydrologic changes that might not be detected when using only one or two spectral bands. Change vector analysis (CVA) is a change detection technique that can measure change in more than two spectral bands, giving it an advantage when mapping rapidly changing and highly diverse wetlands (Baker et al. 2007; Coppin et al. 2004; Mitsch and Gosselink 2000). CVA determines the direction and magnitude of changes in multi-dimensional spectral space (Houhoulis and Michener 2000). CVA concurrently analyzes change in all data layers, instead of a few selected spectral bands (Coppin et al. 2004). The CVA method identifies a change magnitude threshold that is used to separate actual land cover changes from subtle changes due to the variability within land cover classes, as well as radiometric changes associated with instrument and atmospheric variations (Hame et al. 1998; Johnson and Kasischke 1998). Defining spectral threshold values to separate true landscape changes from inherent spectral variation is particularly beneficial for studies of broadly diverse ecosystems, such as wetlands (Houhoulis and Michener 2000). Human interpretation and sometimes an empirical threshold method need to be applied for interpretation of CVA results to obtain accurate information on wetland changes.

1.6 Submerged Aquatic Vegetation (SAV)

Seagrass beds provide essential habitat for many aquatic species, stabilize and enrich sediments, dissipate turbulence, reduce current flow, cycle nutrients, and improve water quality (Hughes et al. 2009). However, in many parts of the world, the health and quantity of seagrass beds has been declining (Orth et al. 2006; Waycott et al. 2009). The decline of coral reefs and SAV is closely linked to human activity since the coastlines and estuaries that host them are often heavily populated. Specifically, the declines have been attributed to reduction in water clarity, alteration of sediment migration via dredging, destruction from coastal engineering, boating and commercial fishing. High concentrations of nutrients exported from agriculture or urban sprawl in coastal watersheds are causing algal blooms in many estuaries and coastal waters (Klemas 2012). Algal blooms are harmful in that they cause eutrophic conditions, depleting oxygen levels needed by organic life and limiting aquatic plant growth by reducing water transparency.

Submerged aquatic plants and their properties are not as easily detectable as terrestrial vegetation. The spectral response of aquatic vegetation resembles that of terrestrial vegetation, yet the submerged or flooded conditions introduce factors that

alter its overall spectral characteristics (Fyfe 2003; Han and Rundquist 2003; Pinnel et al. 2004; Williams et al. 2003). Thus the main challenge for remote sensing of submerged aquatic plants is to isolate the weakened plant signal from the interference of the water column, the bottom and the atmosphere. In addition to bottom reflectance, optically active materials, such as phytoplankton, suspended sediments and dissolved organics, affect the scattering and absorption of the radiation. A careful correction of atmospheric effects is important prior to the analysis of submerged vegetation imagery derived from satellite or high altitude airborne data (Silva et al. 2008).

More recently water column optical models have been used to correct water and bottom effects by including bathymetric information as one of the variables (Dierssen et al. 2003; Heege et al. 2003). Paringit et al. (2003) developed a seagrass canopy model to predict the spectral response of submerged macrophytes in shallow waters. The model considers not only the effects of the water column through radiative transfer modeling, but also viewing and illumination conditions, leaf and bottom reflectance, leaf area index and the vertical distribution of biomass. By inverting the model, the authors were able to estimate plant coverage and abundance with IKONOS satellite imagery, and compare the remotely sensed results with field measurements (Silva et al. 2008). In several other studies digital elevation models and bathymetric data have also been successfully incorporated in the SAV classification approach in order to relate the change in the SAV to water depth (Valta-Hulkkonen et al. 2003, 2004; Wolter et al. 2005).

Since SAV communities have high spatial complexity and temporal variability, standard methods for determining seagrass status and trends have been based on high resolution aerial color photography taken from low to medium altitude flights (Ferguson et al. 1993; NOAA-CSC 2001; Pulich et al. 1997). The color photos are traditionally analyzed by photo-interpreting the 9×9 in. positive photo-transparencies to map the SAV distribution. This is often followed by digitization of the seagrass polygons from map overlays and compilation of digital data into a spatial GIS database. Using airborne color and color infrared video imagery researchers have been able to distinguish between water hyacinth and hydrilla with an accuracy of 87.7 % (Everitt et al. 1999). Good mapping results have also been obtained with recently available airborne digital cameras (Kolasa and Craw 2009).

Large SAV beds and other benthic habitats have been mapped using Landsat TM with limited accuracies ranging from 60 to 74 %. Eight bottom types could be spectrally separated using supervised classification: sand, dispersed communities over sand, dense seagrass, dispersed seagrass over sand, reef communities, mixed vegetation over muddy bottom, and deep water (Gullstrom et al. 2006; Nobi and Thangaradjou 2012; Schweitzer et al. 2005; Wabnitz et al. 2008). SAV biomass has been mapped with Landsat TM using regression analysis between the principal components and biomass, after eigenvector rotation of four TM bands (Armstrong 1993; Zhang 2010). Changes in eelgrass and other seagrass beds have also been mapped with TM data with accuracies of about 66 %, including a study which showed that image differencing was more effective than post-classification or principal component change detection analysis (Macleod and Congalton 1998; Gullstrom et al. 2006).

The mapping of submerged aquatic vegetation (SAV), coral reefs and general bottom characteristics from satellites has become more accurate since high resolution (0.4–4 m) multispectral imagery became available (Mumby and Edwards 2002; Purkis et al. 2002; Purkis 2005). Coral reef ecosystems usually exist in clear water and can be classified to show different forms of coral reef, dead coral, coral rubble, algal cover, sand, lagoons, different densities of seagrasses, *etc*. SAV often grows in somewhat turbid waters and thus is more difficult to map. Aerial hyperspectral scanners and high resolution multispectral satellite imagers, such as IKONOS and QuickBird, have been used to map SAV with accuracies of about 75 % for classes including high-density seagrass, low-density seagrass, and unvegetated bottom (Dierssen et al. 2003; Mishra et al. 2006; Wolter et al. 2005).

Hyperspectral imagers have improved SAV and coral reef mapping results by being able to identify more estuarine and intertidal habitat classes (Garono et al. 2004; Mishra et al. 2006; Phinn et al. 2008; Pu et al. 2012; Purkis et al. 2008; Nayegandhi et al. 2009). Figure 1.2 shows a 2006 hyperspectral image of seagrass communities in the St. Joseph Bay Aquatic Preserve in Florida. The maps produced from such images showed coverage and extent of seagrass communities in the bay, and provided an indicator of the bay's health. The maps were used to identify "good" areas to be targeted for protection, and "poor" areas to be targeted for restoration (CAMA 2009).

SAV has been mapped with high accuracies using airborne hyperspectral imagers and regression models, binary decision trees incorporating spectral mixture analysis, spectral angle mapping, and band indexes (Hestir et al. 2008; Peneva et al. 2008). Airborne LiDARS have also been used with multispectral or hyperspectral imagers to map coral reefs and SAV (Brock et al. 2004, 2006; Brock and Purkis 2009).

Acoustic techniques have been used for rapid detection of submerged aquatic vegetation in turbid waters. The acoustic impedance (density difference between the plant and surrounding water) which produces the reflections, is thought to result primarily from the gas within the plant, since the more buoyant species (with more gas) reflect acoustic signals more strongly. Hydroacoustic techniques include horizontally-aimed side scanning sonar systems and vertically-aimed echo sounders. Side-scan sonar systems provide complete bottom coverage and generate an image. They have been effective for delineating seagrass beds (Moreno et al. 1998; Sabol et al. 2002). The horizontal orientation of the acoustic beam results in a stronger reflected signal from the vertically oriented grass blades.

Echo sounders are pointed vertically downward and traverse a path generating an analog strip chart, with the horizontal axis equal to distance, vertical axis equal to depth, and echo intensity shown as gray scale. Numerous researchers using echo sounders have reported success in detecting and qualitatively characterizing seagrass beds (Miner 1993; Hundley 1994). For instance, Sabol et al. (2002) used high resolution digital echo sounders linked with GPS equipment. The acoustic reflectivity of SAV allowed for detection and measurement of canopy geometry, using digital signal processing algorithms. Comparison with field data showed good detection and measurement performance over a wide range of conditions.

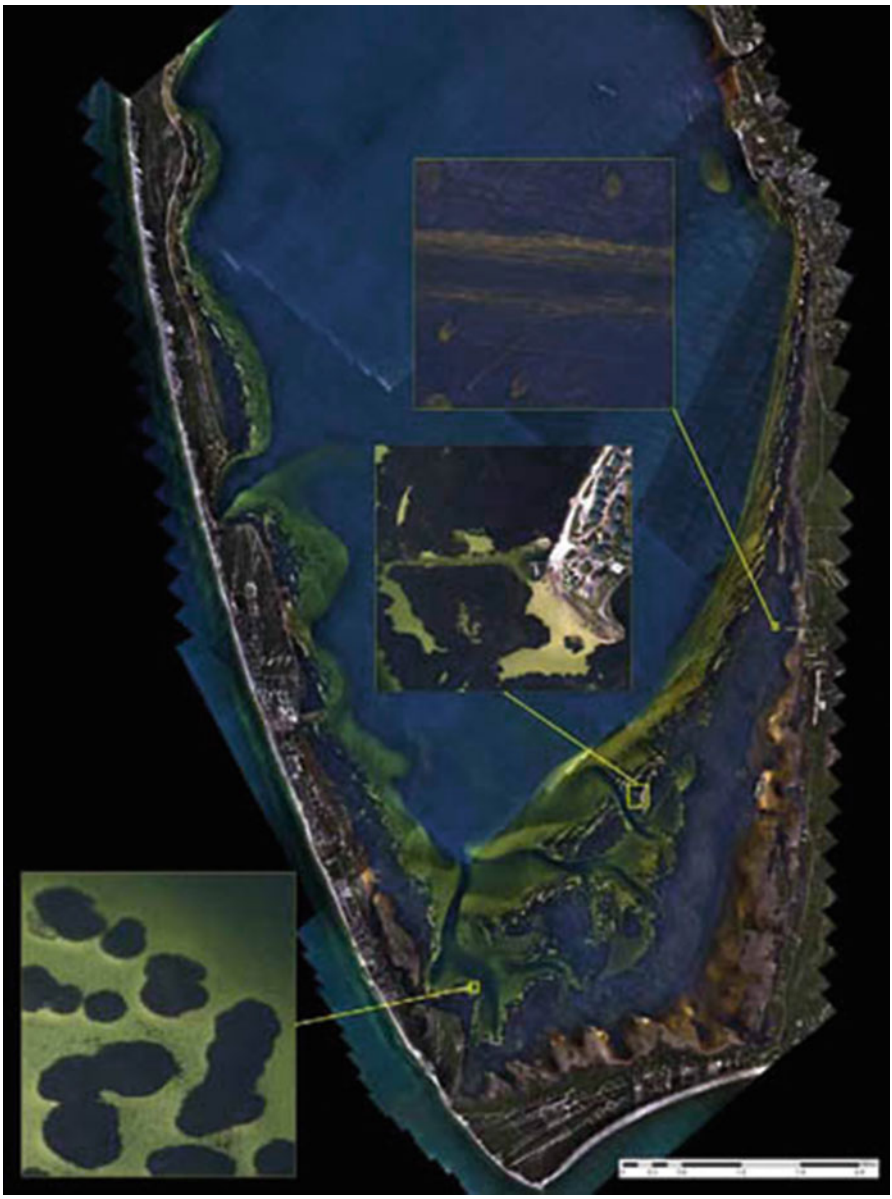

Fig. 1.2 Hyperspectral imagery of seagrass communities in St. Joseph Bay, FL (CAMA 2009)

1.7 Beach Profiling and Shoreline Change Detection

Information on beach profiles and coastal bathymetry is needed for studies of near-shore geomorphology, hydrology and sedimentary processes (Finkl et al. 2005a; Lidz et al. 1997). In order to plan sustainable coastal development

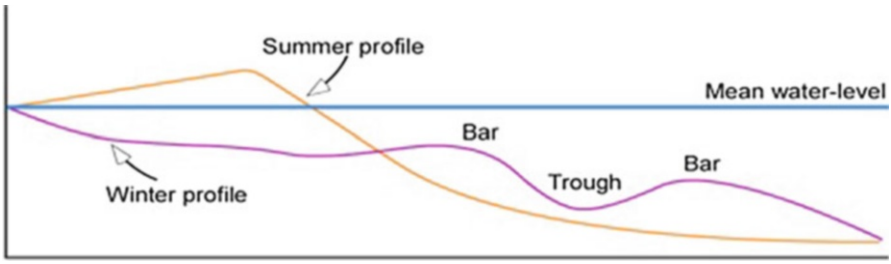

Fig. 1.3 Changes in beach profiles between summer and winter due to changes in wave climate. During winter storms the beach is eroded and seaward cross-shore sediment transport results in the formation of off-shore bars (Purkis and Klemas 2011)

and implement effective beach erosion control, flood zone delineation and ecosystem protection, coastal managers and researchers need information on long-term and short-term changes taking place along the coast, including changes in beach profiles due to erosion by storms and littoral drift, wetlands changes due to inundation, *etc*. (Gesch 2009; West et al. 2001).

Beach profiles and shoreline positions can change rapidly with seasons and after storms, in addition to exhibiting slower changes due to littoral drift and sea level rise (Stockdon et al. 2009). During winter storms waves remove sand from the beach and deposit it offshore, typically in bar formation (Fig. 1.3). During summer, milder wave formations move the bars onshore and rebuild the wider berm for the "summer beach". Long-term changes of shorelines due to littoral drift or sea level rise can be aggravated by man-made structures such as jetties, seawalls and groins (Finkl 1996; Irish and White 1998; Khalil and Finkl 2007; Klemas 2009; Wang 2010).

Before the advent of the Global Positioning System (GPS) and Light Detection and Ranging (LiDAR) systems, shoreline position analysis and beach profiling were based on historical aerial photographs and topographical sheets (Morton and Miller 2005). To map long-term changes of shorelines due to beach erosion, time-series of historical aerial photographs are available dating back to the 1930s and topographic maps exist to extend the record of shoreline change to the mid-late 1800s. Such data are held by local, state and federal agencies, including the U.S. Geological Survey and the USDA Soil Conservation Service. These agencies also have various maps, including planimetric, topographic, quadrangle, thematic, ortho-photo, satellite and digital maps (Jensen 2007; Rasher and Weaver 1990). Time series of high resolution satellite images have also been used to map shoreline changes, but with accuracies of the order of several meters.

To perform a shoreline position analysis, the shoreline can be divided into segments which are uniformly eroding or accreting. Then the change in the distance of the waterline can be measured in reference to some stable feature like a coastal highway. The instantaneous water line in the image is not a temporally representative shoreline. The high water line, also referred to as the wet/dry line, is a commonly used indicator because it is visible in most images. Other indicators include the vegetation line, bluff line, or man-made shore vestments (Boak and Turner 2005; Thieler and Danforth 1994).

Topographical and depth data can now be effectively acquired at various spatial scales by airborne laser surveys using LiDAR techniques (Guenther et al. 1996; Ackermann 1999; Krabill et al. 2000; Lillycrop et al. 2002). A laser transmitter/receiver mounted on an aircraft transmits a laser pulse that travels to the land surface or the air-water interface, where a portion of this energy reflects back to the receiver. The land topography is obtained from the LiDAR pulse travel-time. On water, some of the energy propagates through the water column and reflects off the sea bottom. The water depth is calculated from the time lapse between the surface return and the bottom return (Hapke 2010; Purkis and Klemas 2011).

Global Positioning Systems (GPS), combined with airborne LiDAR techniques, make it now possible to obtain accurate topographical maps, including shoreline positions (Jensen 2007; Morton and Miller 2005; Schmid et al. 2011). A particularly effective approach for studying sand dynamics along coastlines includes the combined use of airborne hyperspectral data and airborne LiDAR data. Airborne LiDAR surveying has been significantly enhanced by kinematic differential GPS methods which enable the positioning of small aircraft to within several centimeters. Inertial navigation systems provide three-dimensional aircraft orientation to within 0.005° making aero-triangulation with ground data points unnecessary. LiDAR transmitters can provide elevation measurements at over 2,000 points per second from altitudes of 500–1,000 m with vertical accuracies of 10–15 cm (Brock and Sallenger 2000; Cracknell and Hayes 2007; Finkl et al. 2005a; Hapke 2010).

A typical beach profiling procedure using LiDAR may include cross-shore profiles every 10 m. Beach slope and location, elevation of the berm, dune base and dune crest can also be determined from these beach profiles. One can use a known vertical datum to remove the subjective nature of identifying the shoreline. The water line is then readily identified, because laser returns from the sea are noisy (Stockdon et al. 2002).

A LiDAR aircraft mapping configuration usually includes a light aircraft equipped with a LiDAR instrument and GPS, which is operated in tandem with a GPS base station. In coastal applications, the aircraft flies along the coast at heights of about 200–500 m, surveying a ground swath directly below the aircraft. The aircraft position throughout the flight is recorded by an onboard GPS receiver. The aircraft GPS signals are later combined with signals concurrently collected by a nearby GPS base station. Differential kinematic GPS post-processing determines the aircraft flight trajectory to within about 5 cm (Cracknell and Hayes 2007; Wang 2010). Although airborne laser mapping may be carried out at night, flight safety dictates that coastal LiDAR operations are normally confined to daylight hours and timed to coincide with low tide to maximize coverage of the beach face.

LiDAR surveys can now produce a 10 cm vertical accuracy at spatial densities greater than one elevation measurement per square meter. Such performance satisfies the needs of various coastal applications, including flood zone delineation, monitoring beach nourishment projects and mapping changes along barrier island beaches and other sandy coasts (Brock and Purkis 2009; Deronde et al. 2006; Gares et al. 2006; Raber et al. 2007; Webster et al. 2004; Wozencraft and Millar 2005). The ability of LiDAR to rapidly survey long, narrow strips of terrain is important,

because beaches are elongate, highly dynamic sedimentary environments that undergo seasonal and long-term erosion or accretion and are also impacted by severe storms (Kempeneers et al. 2009; Krabill et al. 2000; Stockdon et al. 2002; Zhou 2010).

In order to develop digital flood insurance maps and data for habitat studies and vegetation identification, in 2005 the State of Delaware contracted with USGS and NASA to produce high detail elevation data using NASA's Experimental Advanced Airborne Research LiDAR (EAARL), which was specifically designed to measure submerged topography and adjacent coastal land elevations. Emergency managers have been able to use this data to develop statewide inundation maps and to incorporate this data into flood and storm surge models to create an early-flood-warning system (Carter and Scarborough 2010).

1.8 Bathymetry

The lack of accurate near-shore bathymetric data has been identified as a key limitation in the application of geospatial data to coastal environments (Malthus and Mumby 2003). Remote sensing techniques that have been successfully used to map coastal water depth include LiDAR and acoustic depth sounding. In LiDAR bathymetry, a laser transmitter/receiver mounted on an aircraft transmits a pulse that reflects off the air-water interface and the sea bottom. Since the velocity of the light pulse is known, the water depth can be calculated from the time lapse between the surface return and the bottom return. Because laser energy is lost due to refraction, scattering and absorption at the water surface, the sea bottom and inside the water column, these effects limit the strength of the bottom return and limit the maximum detectable depth.

Examples of LiDAR applications include regional mapping of changes along sandy coasts due to storms or long-term sedimentary processes and in the analysis of shallow benthic environments (Bonisteel et al. 2009; Guenther et al. 1996; Irish and Lillycrop 1997; Gutierrez et al. 1998; Kempeneers et al. 2009; Sallenger et al. 1999). Bertels et al. (2012) used integrated optical and acoustic remote sensing data over the backshore-foreshore-nearshore continuum to study sediment dynamics along the Belgian coastline. To accomplish this, the authors combined airborne hyperspectral imaging spectroscopy, airbore laser scanning and seaborne sonar. The LiDAR and hyperspectral data were combined with side-scan sonar and single- and multibeam depth and backscatter data to construct integrated sedimentological and morphological maps (Bertels et al. 2012).

Another example is the use of airborne laser bathymetry (ALB) to rapidly acquire large, high-quality data sets along the Continental Shelf of southeast Florida by Finkl et al. (2005b). The ALB provided a contiguous set of data for 160 km of coast from onshore to 6 km offshore. Image enhancement of the ALB digital data facilitated recognition of numerous seafloor features and bathymetric patterns. Bathymetric analysis of the 600 sq km survey area allowed for the first time an

assessment of links between the influence of seabed morphology on wave transformation patterns and beach morphodynamics in southeast Florida.

To maximize water penetration, bathymetric LiDARs employ a blue-green laser with a typical wavelength of 530 nm to range the distance to the seabed. With the near-exponential attenuation of electromagnetic energy by water with increasing wavelength, a pure blue laser with a wavelength shorter than 500 nm would offer greater penetration. However, this wavelength is not used because, first, blue light interacts much more strongly with the atmosphere than longer wavelengths; and second, creating a high-intensity blue laser is energetically less efficient than blue-green and consumes a disproportionately large amount of instrument power.

Conversely, terrestrial topographical LiDARs typically utilize near-infrared (NIR) lasers with wavelengths of 1,064 nm. As is the case for the blue-green laser used for hydrography, this NIR wavelength is focused and easily absorbed by the eye. Therefore, the maximum power of the LiDAR system is limited by the need to make them eye-safe. While bathymetric lasers are limited in their accuracy by water column absorption, terrestrial infrared lasers suffer from null or poor returns from certain materials and surfaces such as water, asphalt, tar, clouds and fog, all of which absorb NIR wavelengths.

Because they do not penetrate water predictably, NIR topographical lasers cannot be used to assess bathymetry. Dual-wavelength LiDAR provides both bathymetric and topographical LiDAR mapping capability by carrying both an NIR and a blue-green laser. The NIR laser is not redundant over water, because it reflects off the air-water interface and can be used to refine the altitude above the sea surface as well as to distinguish dry land from water using the signal polarization (Guenther 2007). In addition, specific LiDAR systems, like the Scanning Hydrographic Operational Airborne LiDAR System (SHOALS), record the red wavelength Raman signal (647 nm). The Raman signal comes from interactions between the blue-green laser and water molecules, causing part of the energy to be backscattered while changing wavelength (Guenther et al. 1994; Irish and Lillycrop 1999). A detailed description of the SHOALS system is provided by Lillycrop et al. (1997).

By employing a very high scan-rate, state-of-the-art systems such as the Experimental Advanced Airborne Research LiDAR (EAARL) have been used to measure both, topography and bathymetry, from the return time of a single blue-green laser (Bonisteel et al. 2009; McKean et al. 2009; Nayegandhi et al. 2009). Operating in the blue-green portion of the electromagnetic spectrum, the EAARL is specifically designed to measure submerged topography and adjacent coastal land elevations seamlessly in a single scan of transmitted laser pulses. Figure 1.4 shows such a bathymetric-topographical DEM of a section of the Assateague Island National Seashore, captured by the EAARL. Assateague Island National Seashore consists of a 37-mile-long barrier island along the Atlantic coasts of Maryland and Virginia. This experimental advance signaled the future move towards commercial implementation of dual-application but single-wavelength instruments (Krabill et al. 2000; Wozencraft and Lillycrop 2003).

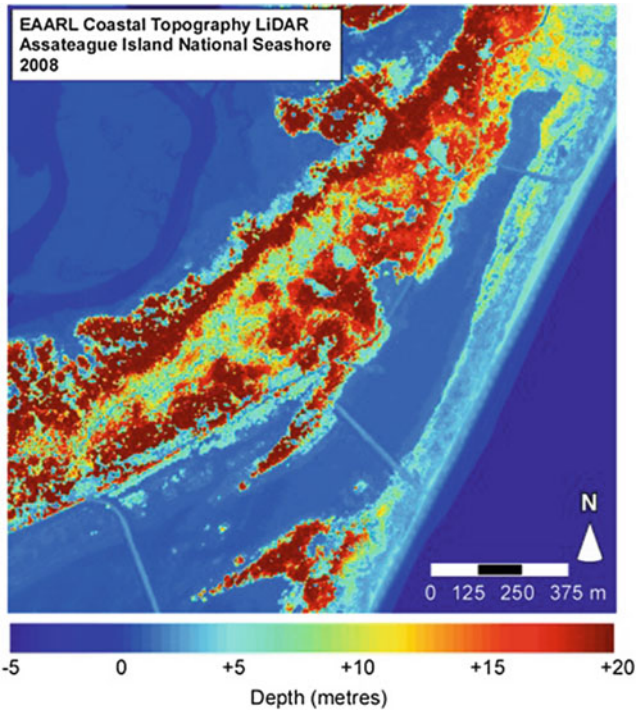

Fig. 1.4 Coastal topography for a section of the Assateague Island National Seashore acquired using the Experimental Advanced Airborne Research LiDAR (EAARL) (Bonisteel et al. 2009) (Credit: USGS)

While the EAARL and dual-wavelength LiDARs offer nearly seamless profiles between bathymetry and terrestrial terrain, neither bathymetric system can acquire dependable bathymetric data in very shallow depths or over white water in the surf zone. When white-caps are present, the laser does not penetrate the water column. Furthermore, if the depth is less than 2 m, even in clear water it becomes difficult to separate the laser pulse returning from the water surface from the one reflected by the bottom bed (Parson et al. 1997; Philpot 2007; Bonisteel et al. 2009). For coastal mapping, both problems are obviated by combining successive flights at low tide with a topographical LiDAR, and at high tide with a bathymetric LiDAR (Pastol et al. 2007; Sinclair 2008; Stoker et al. 2009). Such a strategy is not possible for coastal areas that do not have large tidal variations, or for non-tidal inland water bodies.

Optical water clarity is the most limiting factor for LiDAR depth detection, so it is important to conduct the LiDAR overflights during tidal and current conditions that minimize the water turbidity due to sediment re-suspension and river inflow (Sinclair 2008). LiDAR overflights should not be conducted during high wind conditions, since the rough water surface will scatter the LiDAR pulse and make it difficult to detect (Brock and Sallenger 2000; Irish and Lillycrop 1999).

Table 1.1 LiDAR flight parameters

Flying height	200–500 m (400 m typical)
Vertical accuracy	±15 cm
Horizontal accuracy	DGPS = 3 m; KGPS = 1 m
Max mapping depth	60 m (clear water)
Typical *kd* product	4
Coastal *k*	0.2–0.8 (d = 5–20 m)
Estuarine *k*	1.0–4.0 (d = 1–4 m)
Sounding density	3–15 m
Sun angle	18°–25° (to minimize glare)
Scan geometry	Circular (220 m swath typical)
Sea state	Low (0–1 Beaufort scale)
Water penetration	Green LiDAR (532 nm) used
Aircraft height	Infrared LiDAR (1,064 nm) used

DGPS differential GPS mode, *KGPS* kinematic GPS mode

Typical flight parameters for airborne LiDARs used in bathymetry are shown in Table 1.1. The LiDAR system must have a *kd* factor large enough to accommodate the water depth and water turbidity at the study site (k = attenuation coefficient; d = max. water penetration depth). For instance, if a given LiDAR system has a $kd = 4$ and the turbid water has an attenuation coefficient of $k = 1$, the system will be effective only to depths of approximately 4 m. Typically, a LiDAR sensor may collect data down to depths of about three times the Secchi (visible) depth (Estep et al. 1994; Sinclair 2008). Beyond that depth, one may have to use acoustic echo-sounding profilers or side-scan imaging sonars (Brock and Sallenger 2000).

Echo-sounding profilers, which measure water depth and changes in bottom topography, send out pulses of acoustic energy from beneath the boat or other platform. The acoustic "ping" is reflected off the seabottom and submerged objects and recorded by the transceiver. The depth to target calculation is based on how long it took the reflected pulse to return to the surface and the speed of sound in water under prevailing environmental conditions. The earliest sounders used single beams, but the newer systems use multiple beams, with a large array of beams measuring bottom depths across a wide swath (Bergeron et al. 2007; Cracknell and Hayes 2007).

Side-scan imaging sonars emit acoustic pulses in the form of a very wide fan-shaped beam to both sides and at right angles to the track, to produce an image of the seabottom from the backscattered acoustic energy. Sonar echo-sounders and side-scan sonars are frequently housed in a torpedo-shaped "fish", which is towed by cable behind the survey ship at a predetermined height off the bottom (Avery and Berlin 1992; Pittenger 1989; Thompson and Schroeder 2010). More recently, various acoustic sensors have been housed in Remotely Operated Vehicles (ROVs) or Autonomous Underwater Vehicles (AUV's) and used to monitor features on the bottom and in the water column (Chadwick 2010).

1.9 Summary and Conclusions

Coastal ecosystems are highly productive and act as critical habitats for a wide variety of plants, fish, shellfish, and other wildlife. Coastal wetlands and estuaries have been exposed to a wide range of natural and man-induced alterations, including dredge and fill operations, hydrologic modifications, pollutant run-off, eutrophication, impoundments and fragmentation by roads and ditches. Environmental impacts from sea level rise and more frequent coastal storms are causing increased beach erosion, wetland destruction, algal blooms, hypoxia and anoxia, fish kills, releases of pollutants, and spread of pathogens.

Since coastal ecosystems have high spatial complexity and temporal variability, they require high spatial, spectral and temporal resolutions. Advances in sensor design and data analysis techniques are making remote sensing systems attractive for monitoring and mapping changes in the coastal zone. High resolution multispectral and hyperspectral imagers, LiDAR and radar systems are available for monitoring changes in coastal marshes, submerged aquatic vegetation, coral reefs, and beach profiles. Imaging radars are sensitive to soil moisture and inundation and can detect hydrologic features beneath the vegetation canopy.

Submerged aquatic plants and their properties are not as easily detectable as terrestrial vegetation. The main challenge for remote sensing of submerged aquatic plants is to isolate the weakened plant signal from the interference of the water column, the bottom and the atmosphere. Airborne hyperspectral imagers have improved SAV and coral reef mapping results by being able to identify more estuarine and intertidal habitat classes. The mapping of submerged aquatic vegetation (SAV), coral reefs and general bottom characteristics from satellites has become more accurate since high resolution multispectral imagery became available.

To identify long-term trends and short term variations, such as the impact of rising sea levels and hurricanes on wetlands, one needs to analyze time-series of remotely sensed imagery. High temporal resolution, precise spectral bandwidths, and accurate georeferencing procedures are factors that contribute to the frequent use of satellite image data for change detection analysis. Detecting the actual changes between two registered and radiometrically corrected images from different dates can be accomplished by employing one of several techniques, including post-classification comparison (PCC), spectral image differencing (SID), and change vector analysis (CVA). A comparison of the SID and the PCC change detection algorithms is provided by Macleod and Congalton (1998).

Global Positioning Systems (GPS), combined with airborne LiDAR techniques, make it now possible to obtain accurate topographical maps, including shoreline positions. LiDAR surveys can produce a 10 cm vertical accuracy at spatial densities greater than one elevation measurement per square meter. Such performance satisfies the needs of most coastal applications. Airborne LiDAR and ship-borne acoustic depth profilers are being used to map coastal water depth and bottom topography. LiDAR profilers, employing blue-green lasers, can penetrate the water column down to depths of about three times the Secchi depth.

Remote sensors can monitor and assess long-term trends and short-term changes of vegetation and hydrology faster, more completely and at lower cost per unit area than field or ship surveys alone. Multi-sensor and multi-seasonal data fusion techniques are significantly improving coastal land cover mapping accuracy and efficiency. Combinations of different satellite and airborne sensors can provide data that enhances the research and management of coastal ecosystems.

Future research priorities should include investigations of best approaches for processing hyperspectral data. Hyperspectral sensors need to be tested for SAV and bottom type discrimination using data obtained from satellites. The question of how differing levels of tidal inundation affect the reflectance characteristics of emergent marsh vegetation still needs to be better documented. Finally there is a need to investigate improvements to be gained from synergistic use of multi-wavelength remote sensing approaches, change detection techniques and multi-temporal comparisons and knowledge-based methods for improving classification accuracy (Malthus and Mumby 2003).

References

Ackermann F (1999) Airborne laser scanning – present status and future expectations. ISPRS J Photogramm Remote Sen 54:64–67

Adam E, Mutanga O, Rugege D (2010) Multispectral and hyperspectral remote sensing for identification and mapping of wetland vegetation: a review. Wet Ecol Manag 18:281–296

Armstrong RA (1993) Remote sensing of submerged vegetation canopies for biomass estimation. Int J Remote Sens 14:621–627

Artigas FJ, Yang J (2006) Spectral discrimination of marsh vegetation types in the New Jersey meadowlands, USA. Wetlands 26:271–277

Avery TE, Berlin GL (1992) Fundamentals of remote sensing and airphoto interpretation. Macmillan Publishing Company, New York

Baghdadi N, Bernier M, Gauthier R, Neeson I (2001) Evaluation of C-band SAR data for wetlands mapping. Int J Remote Sens 22:71–88

Baker C, Lawrence RL, Montagne C, Patten D (2007) Change detection of wetland ecosystems using Landsat imagery and change vector analysis. Wetlands 27:610–619

Bergeron E, Worley CR, O'Brien T (2007) Progress in the development of shallow water mapping systems. Sea Technol 48:10–15

Bertels L, Houthuys R, Deronde B, Janssens R, Verfaillie E, Van Lancker V (2012) Integration of optical and acoustic remote sensing data over the backshore-foreshore-nearshore continuum: a case study in Ostend (Belgium). J Coast Res 28:1426–1436 (in press)

Blasco F, Aizpuru M, Din Ndongo D (2005) Mangroves remote sensing. In: Schwartz ML (ed) Encyclopedia of coastal science. Springer, Dordrecht, pp 614–617

Boak EH, Turner IL (2005) Shoreline definition and detection: a review. J Coast Res 21:688–703

Bonisteel JM, Nayegandhi A, Wright CW, Brock JC, Nagle DB (2009) Experimental Advanced Airborne Research LiDAR (EAARL) data processing manual. US Geological Survey Open-File Report, 2009-1078

Bourgeau-Chavez LL, Kasischke ES, Brunzell SM, Mudd JP, Smith KB, Frick AL (2001) Analysis of space-borne SAR data for wetland mapping in Virginia riparian ecosystems. Int J Remote Sens 22:3665–3687

Brock J, Sallenger A (2000) Airborne topographic mapping for coastal science and resource management. USGS Open-File Report 01–46

Brock JC, Purkis SJ (2009) The emerging role of LiDAR remote sensing in coastal research and resource management. J Coast Res 53:1–5, Special issue 53, Coastal Applications of Airborne LiDAR

Brock JC, Wright CW, Clayton TD, Nayegandhi A (2004) LIDAR optical rugosity of coral reefs in Biscayne National Park, Florida. Coral Reefs 23:48–59

Brock J, Wright CW, Hernandez R, Thompson P (2006) Airborne LiDAR sensing of massive stony coral colonies on patch reefs in the northern Florida reef tract. Remote Sens Environ 104:31–42

Bustamante J, Pacios F, Diaz-Delgado R, Aragones D (2009) Predictive models of turbidity and water depth in the Donana marshes using Landsat TM and ETM+ images. J Environ Manage 90:2219–2225

CAMA (2009) Mapping and monitoring seagrass communities. Office of Coastal and Aquatic Management Areas, Florida Department of Environmental Protection. Available online at: http://www.dep.state.fl.us/coastal/habitats/seagrass/management/mapping.htm. Accessed 21 June 2012

Carter D, Scarborough R (2010) Sharing Delaware's lidar lessons. NOAA Coastal Services Center report. Local Strateg Addressing Clim Chang 2:16–17

Chadwick W (2010) Remotely Operated Vehicles (ROVs) and Autonomous Underwater Vehicles (AUVs). NOAA Ocean Explorer: submarine ring of fire 2002: Background. http://oceanexplorer.noaa.gov/explorations/02fire/background/rovsauvs/rov_auv.html

Christian B, Krishnayya NSR (2009) Classification of tropical trees growing in a sanctuary using Hyperion (EO-1) and SAM algorithm. Curr Sci 96:1601–1607

Coppin P, Jonckhere I, Nackaerts K, Mays B, Lambin E (2004) Digital change detection methods in ecosystem monitoring: a review. Int J Remote Sens 25:1565–1596

Costa MPF, Telmer KH (2007) Mapping and monitoring lakes in the Brazilian Pantanal wetland using synthetic aperture radar imagery. Aquat Conserv Mar Freshw Ecosyst 17:277–288

Cracknell AP, Hayes L (2007) Introduction to remote sensing. CRC Press, New York

Dahl TE (2006) Status and trends of wetlands in the conterminous United States 1998 to 2004. U.S. Department of the Interior, Fish and Wildlife Service Publication, Washington, DC, p 112

Deronde B, Houthuys R, Debruyn W, Fransaer D, Lancker VV, Hernriet J-P (2006) Use of airborne hyperspectral data and laser scan data to study beach morphodynamics along the Belgian coast. J Coast Res 22:1108–1117

Dierssen HM, Zimmermann RC, Leathers RA, Downes V, Davis CO (2003) Ocean color remote sensing of seagrass and bathymetry in the Bahamas banks by high resolution airborne imagery. Limnol Oceanogr 48:444–455

Dwivedi R, Rao B, Bhattacharya S (1999) Mapping wetlands of the Sundarban Delta and it's environs using ERS-1 SAR data. Int J Remote Sens 20:2235–2247

Ellis JM, Dodd HS (2000) Applications and lessons learned with airborne multispectral imaging. In: Fourteenth International Conference on Applied Geologic Remote Sensing, Las Vegas, NV

Estep LL, Lillycrop WJ, Parson LE (1994) Estimation of maximum depth of penetration of a bathymetric lidar system using a Secchi depth data base. Mar Technol Soc J 28:31–36

Everitt JH, Yang C, Escobar DE, Webster CF, Lonard RI, Davis MR (1999) Using remote sensing and spatial information technologies to detect and map two aquatic macrophytes. J Aquat Plant Manag 37:71–80

Fearns PRC, Klonowski W, Babcock RC, England P, Phillips J (2011) Shallow water substrate mapping using hyperspectral remote sensing. Cont Shelf Res 31:1249–1259

Ferguson RL, Wood LL, Graham DB (1993) Monitoring spatial change in seagrass habitat with aerial photography. Photogramm Eng Remote Sens 59:1033–1038

Filippi AM, Jensen JR (2006) Fuzzy learning vector quantization for hyperspectral coastal vegetation classification. Remote Sens Environ 100:512–530

Finkl CW (1996) What might happen to America's shorelines if artificial beach replenishment is curtailed: a prognosis for southeastern Florida and other sandy regions along regressive coasts. J Coast Res 12:ii–ix

Finkl CW, Benedet L, Andrews JL (2005a) Interpretation of seabed geomorphology based on spatial analysis of high-density airborne laser bathymetry (ALB). J Coast Res 21:501–514

Finkl CW, Benedet L, Andrews JL (2005b) Submarine geomorphology of the continental shelf off southeast Florida based on interpretation of airborne laser bathymetry. J Coast Res 21:1178–1190

Fyfe SK (2003) Are seagrasses spectrally distinct? Limnol Oceanogr 48:464–479

Gares PA, Wang Y, White SA (2006) Using Lidar to monitor a beach nourishment project at Wrightsville Beach, North Carolina, USA. J Coast Res 22:1206–1219

Garono RJ, Simenstad CA, Robinson R, Ripley H (2004) Using high spatial resolution hyperspectral imagery to map intertidal habitat structure in Hood Canal Washington, USA. Can J Remote Sens 30:54–63

Gesch DB (2009) Analysis of Lidar elevation data for improved identification and delineation of lands vulnerable to sea-level rise. J Coast Res 49–58, Special issue 53, Coastal Applications of Airborne Lidar

Ghioca-Robrecht DM, Johnston CA, Tulbure MG (2008) Assessing the use of multiseason QuickBird imagery for mapping invasive species in Great Lakes coastal marsh. Wetlands 28:1028–1039

Gilmore MS, Civco DL, Wilson EH, Barrett N, Prisloe S, Hurd JD, Chadwick C (2010) Remote sensing and in situ measurements for delineation and assessment of coastal marshes and their constituent species. In: Wang J (ed) Remote sensing of coastal environment. Springer, Boca Raton

Guenther G (2007) Airborne LiDAR bathymetry digital elevation. Model technologies and applications. In: Maune D (ed) The DEM users manual. American Society for Photogrammetry and Remote Sensing, pp 253–320

Guenther G, Larocque P, Lillycrop W (1994) Multiple surface channels in SHOALS airborne LiDAR. SPIE Ocean Opt XII 2258:422–430

Guenther GC, Tomas RWL, Larocque PE (1996) Design considerations for achieving high accuracy with the SHOALS bathymetric LiDAR system. SPIE: Laser Remote Sens Nat Waters From Theory Pract 15:54–71

Gullstrom M, Lunden B, Bodin M, Kangwe J, Ohman MC, Mtolera SP, Bjork M (2006) Assessment of changes in the seagrass-dominated submerged vegetation of tropical Chwaka Bay (Zanzibar) using satellite remote sensing. Estuar Coast Shelf Sci 67:399–408

Gutierrez R, Gibeaut JC, Crawford MM, Mahoney MP, Smith S, Gutelius W, Carswell D, Macpherson E (1998) Airborne laser swath mapping of Galveston Island and Bolivar Peninsula, Texas. In: Proceedings of the fifth international conference on remote sensing for marine and coastal environments, San Diego, 1, 236–243

Hame TI, Heiler I, Miguel-Ayanz JS (1998) An unsupervised change detection and recognition system for forestry. Int J Remote Sens 19:1079–1099

Han L, Rundquist D (2003) The spectral responses of *Ceratophyllum demersum* at varying depths in an experimental tank. Int J Remote Sens 24:859–864

Hapke CJ (2010) Integration of LiDAR and historical maps to measure coastal change on a variety of time and spatial scales. In: Wang Y (ed) Remote sensing of coastal environments. Springer/CRC Press, Boca Raton

Harris J, Digby-Argus S (1986) The detection of wetlands on radar imagery. In: Proceedings of the tenth Canadian symposium on remote sensing Edmonton, AB

Harvey KR, Hill JE (2001) Vegetation mapping of a tropical freshwater swamp in the Northern Territory, Australia: a comparison of aerial photography, Landsat TM and SPOT satellite imagery. Remote Sens Environ 22:2911–2925

Heege T, Bogner A, Pinnel N (2003) Mapping of submerged aquatic vegetation with a physically based process chain. SPIE Proc Remote Sens 5233:8

Hess L, Melack J, Simonett D (1990) Radar detection of flooding beneath the forest canopy: a review. Int J Remote Sens 11:1313–1325

Hess L, Melack J, Filoso S, Wang Y (1995) Delineation of inundated area and vegetation along the Amazon floodplain with the SIR-C synthetic aperture radar. IEEE Trans Geosci Remote Sens 33:896–904

Hestir EL, Khanna S, Andrew ME, Santos MJ, Viers JH, Greenberg JA, Rajapakse SS, Ustin S (2008) Identification of invasive vegetation using hyperspectral remote sensing in the California Delta ecosystem. Remote Sens Environ 112:4034–4047
Heumann BW (2011) Satellite remote sensing of mangrove forests: recent advances and future opportunities. Prog Phys Geogr 35:87–108
Hirano A, Madden M, Welch R (2003) Hyperspectral image data for mapping wetland vegetation. Wetlands 23:436–448
Houhoulis P, Michener W (2000) Detecting wetland change: a rule-based approach using NWI and SPOT-XS data. Photogramm Eng Remote Sens 66:205–211
Hundley A (1994) Report on the use of an acoustic method for mapping seagrass density and location. Report no. 940401. Offshore Scientific Services, Sydney
Hughes AR, Williams SL, Duarte CM, Heck KL Jr, Waycott M (2009) Associations of concern: declining seagrasses and threatened dependent species. Front Ecol Environ 7:242–246
Intergovernmental Panel on Climate Change (2007) Climate change 2007: the physical science basis. WMO/UNEP, Paris, www.ipcc.ch
Irish JL, Lillycrop WJ (1997) Monitoring new pass, Florida, with high-density LiDAR bathymetry. J Coast Res 13:1130–1140
Irish JL, Lillycrop WJ (1999) Scanning laser mapping of the coastal zone: the SHOALS system. ISPRS J Photogram Remote Sens 54:123–129
Irish JL, White TE (1998) Coastal engineering applications of high resolution bathymetry. Coast Eng 35:47–71
Jensen JR (1996) Introductory digital image processing: a remote sensing perspective, 2nd edn. Pearson Prentice-Hall, Upper Saddle River
Jensen JR (2007) Remote sensing of the environment: an earth resource perspective. Pearson Prentice-Hall, Upper Saddle River
Jensen RR, Mausel P, Dias N, Gonser R, Yang C, Everitt J, Fletcher R (2007) Spectral analysis of coastal vegetation and land cover using AISA+ hyperspectral data. Geocarto Int 22:17–28
Johnson RD, Kasischke ES (1998) Change vector analysis: a technique for the multispectral monitoring of land cover and condition. Int J Remote Sens 19:411–426
Kasischke E, Bourgeau-Chavez L (1997) Monitoring South Florida wetlands using ERS-1 SAR imagery. Photogramm Eng Remote Sens 63:281–291
Kasischke E, Bourgeau-Chavez L, Smith K, Romanowicz E, Richardson C (1997a) Monitoring hydropatterns in South Florida ecosystems using ERS SAR data. In: 3rd ERS symposium on space at the service of our environment, Florence, pp 71–76
Kasischke E, Melack J, Dobson M (1997b) The use of imaging radars for ecological applications-a review. Remote Sens Environ 59:141–156
Kelly M, Tuxen K (2009) Remote sensing support for tidal wetland vegetation research and management. In: Yang X (ed) Remote sensing and geospatial technologies for coastal ecosystem assessment and management. Springer, Berlin
Kempeneers P, Deronde B, Provoost S, Houthuys R (2009) Synergy of airborne digital camera and LiDAR data to map coastal dune vegetation. J Coast Res 53:73–82
Khalil SM, Finkl CW (2007) Submarine geomorphology and coastal process zones: morphodynamics of the inner continental shelf off southeast Florida. J Coast Res 50:480–485 (special issue)
Klemas V (2009) The role of remote sensing in predicting and determining coastal storm impacts. J Coast Res 25:1264–1275
Klemas V (2011) Remote sensing of wetlands: case studies comparing practical techniques. J Coast Res 27:418–427
Klemas V (2012) Remote sensing of algal blooms: an overview with case studies. J Coast Res 28:34–43
Kolasa KV, Craw V (2009) Improving seagrass maps of Florida's Springs Coast through digital imagery. Proceedings of ASPRS 2009 annual conference, Baltimore, MD, 9–13 Mar 2009
Krabill WB, Wright CW, Swift RN, Frederick EB, Manizade SS, Yungel JK, Martin CF, Sonntag JG, Duffy M, Hulslander W, Brock JC (2000) Airborne laser mapping of Assateague National Seashore Beach. Photogramm Eng Remote Sens 66:65–71

Laba M, Downs R, Smith S, Welsh S, Neider C, White S, Richmond M, Philpot W, Baveye P (2008) Mapping invasive wetland plants in the Hudson River National Estuarine Research Reserve using Quickbird satellite imagery. Remote Sens Environ 112:286–300

Lang MW, Kasischke ES (2008) Using C-band synthetic aperture radar data to monitor forested wetland hydrology in Maryland's Coastal Plain, USA. IEEE Trans Geosci Remote Sens 46:535–546

Lang MW, Mccarty GW (2008) Remote sensing data for regional wetland mapping in the United States: trends and future prospects. In: Russo RE (ed) Wetlands: ecology, conservation and restoration. Nova Science Publishers, Inc., Hauppauge

Lathrop RG, Cole MB, Showalter RD (2000) Quantifying the habitat structure and spatial pattern of New Jersey (U.S.A.) salt marshes under different management regimes. Wetl Ecol Manag 8:163–172

Lesser MP, Mobley CD (2007) Bathymetry, water optical properties, and benthic classification of coral reefs using hyperspectral remote sensing imagery. Coral Reefs 26:819–829

Li L, Ustin SL, Lay M (2005) Application of multiple endmember spectral mixture analysis (MESMA) to AVIRIS imagery for coastal salt marsh mapping: a case study in China Camp, CA, USA. Int J Remote Sens 26:5193–5207

Lidz BH, Shinn EA, Hine AC, Locker SD (1997) Contrasts within an outlier-reef system: evidence for differential quaternary evolution, south Florida windward margin, U.S.A. J Coast Res 13 (3):711–731

Lillycrop WJ, Irish JL, Parson LE (1997) SHOALS system. Sea Technol 38:17–25

Lillycrop WJ, Pope RW, Wozencraft JM (2002) Airborne lidar hydrography: a vision for tomorrow. Sea Technol 43:27–34

Lopez RD, Edmonds CM, Slonecker TS, Jones KB, Heggem DT, Lyon JG, Jaworski E, Garofalo D, Williams D (2004) Accuracy assessment of airborne hyperspectral data for mapping opportunistic plant species in freshwater coastal wetlands. In: Lunetta RS, Lyon JG (eds) Remote sensing and GIS accuracy assessment. CRC Press, New York, pp 253–267

Lunetta RS, Balogh ME (1999) Application of multi-temporal Landsat 5 TM imagery for wetland identification. Photogramm Eng Remote Sens 65:1303–1310

Lunetta RS, Elvidge CD (1998) Remote sensing change detection: environmental monitoring methods and applications. Ann Arbor Press, Ann Arbor

Lyon JG, Mccarthy J (1995) Wetland and environmental applications of GIS. Lewis Publishers, New York

Macleod RD, Congalton RG (1998) A quantitative comparison of change detection algorithms for monitoring eelgrass from remotely sensed data. Photogramm Eng Remote Sens 64:207–216

Malthus TJ, Mumby PJ (2003) Remote sensing of the coastal zone: an overview and priorities for future research. Int J Remote Sens 24:2805–2815

Martin S (2004) An introduction to remote sensing. Cambridge University Press, Cambridge, UK

Martinez JM, Le Toan T (2007) Mapping of flood dynamics and spatial distribution of vegetation in the Amazon floodplain using multitemporal SAR data. Remote Sens Environ 108:209–223

Mccoy R (2005) Field methods in remote sensing. Guilford Press, New York

Mckean J, Nagel D, Tonina D, Bailey P, Wright CW, Bohn C, Nayegandhi A (2009) Remote sensing of channels and riparian zones with a narrow-beam aquatic-terrestrial LiDAR. Remote Sens 1:1065–1096

Miner SP (1993) Application of acoustic hydrosurvey technology to the mapping of eelgrass (Zostera marina) distribution in Humboldt Bay, California. Coastal Zone '93. Proceedings of the 8th symposium on coastal and ocean management, 19–23 July 1993, New Orleans, LA

Mishra D, Narumalani S, Rundquist D, Lawson M (2006) Benthic habitat mapping in tropical marine environments using QuickBird multispectral data. Photogramm Eng Remote Sens 72:1037–1048

Mitsch WJ, Gosselink JG (2000) The value of wetlands: importance of scale and landscape setting. Ecol Econ 35:25–33

Moreno A, Siljestrom P, Rey J (1998) Benthicphanerogam species recognition in side scan sonar images: importance of the sensor direction. In: Alippi A, Cannelli GB (eds) Proceedings 4th European conference on underwater acoustics. Italian National research Council, Rome, pp 173–178

Morris JT, Sundareshwar PV, Nietch CT, Kjerfve B, Cahoon DR (2002) Responses of coastal wetlands to rising sea level. Ecology 83:2869–2877

Morton RA, Miller TL (2005) National assessment of shoreline change: Part 2. Historical shoreline change and associated coastal land loss along the US southeast Atlantic coast. US Geological Survey Open-File Report 2005-1401

Mumby PJ, Edwards AJ (2002) Mapping marine environments with IKONOS imagery: enhanced spatial resolution can deliver greater thematic accuracy. Remote Sens Environ 82:248–257

NASA/GSFC (2010) Hurricane Ike: storm surge flooding image of the Gulf Coast. NASA image courtesy Jeff Schmaltz, MODIS Rapid Response team at NASA GSFC

Nayegandhi A, Brock JC, Wright CW (2009) Small-footprint, waveform-resolving LiDAR estimation of submerged and sub-canopy topography in coastal environments. Int J Remote Sens 30:861–878

NOAA (1999) Trends in U.S. coastal regions, 1970–1998. Addendum to the Proceedings: trends, and future challenges for U.S. National Ocean and Coastal Policy. NOAA, August 1999

NOAA-CSC (2001) Guidance for Benthic Habitat mapping: an aerial photographic approach (by M. Finkbeiner, W. Stevenson, and R. Seaman, NOAA-CSC, Charleston, SC). NOAA/CSC/20117-PUB, 73 pp

Nobi EP, Thangaradjou T (2012) Evaluation of the spatial changes in seagrass cover in the lagoons of Lakshadweep islands, India, using IRS LISS III satellite images. Geocarto Int 27:647–660

Novo EMLM, Costa MPF, Mantovani JE, Lima IBT (2002) Relationship between macrophyte stand variables and radar backscatter at L and C band, Tucurui reservoir, Brazil. Int J Remote Sens 23:1241–1260

Odum EP (1993) Ecology and our endangered life-support systems, 2nd edn. Sinauer Associates, Inc., Sunderland

Orth RJ, Carruthers TJB, Dennison WC, Duarte CM, Fourqurean JW, Heck KL Jr, Hughes AR, Kendrick GA, Kenworthy WJ, Olyarnik S, Short FT, Waycott M, Williams SL (2006) A global crisis for seagrass ecosystems. Bioscience 56:987–996

Ozesmi SL, Bauer ME (2002) Satellite remote sensing of wetlands. Wetl Ecol Manag 10:381–402

Paringit EC, Nadaoka K, Fortes MD, Harii S, Tamura H, Mistui J (2003) Multiangular and hyperspectral reflectance modeling of seagrass beds for remote sensing studies. In: Proceedings of the international geoscience and remote sensing symposium '03, vol 3, pp 21–25, New York: IEEE

Parson LE, Lillycrop WJ, Klein CJ, Ives RC, Orlando SP (1997) Use of LiDAR technology for collecting shallow bathymetry of Florida Bay. J Coast Res 13:1173–1180

Pastol Y, Le Roux C, Louvart L (2007) LITTO3D: a seamless digital terrain model. Int Hydrogr Rev 8:38–44

Peneva EI, Griffith JA, Carter GA (2008) Seagrass mapping in the Northern Gulf of Mexico using airborne hyperspectral imagery: a comparison of classification methods. J Coast Res 24:850–856

Pengra BW, Johnston CA, Loveland TR (2007) Mapping an invasive plant, Phragmitesaustralis, in coastal wetlands using the EO-! Hyperion hyperspectral sensor. Remote Sens Environ 108:74–81

Philpot W (2007) Estimating atmospheric transmission and surface reflectance from a glint-contaminated spectral image. IEEE Trans Geosci Remote Sens 45:448–457

Phinn S, Hess LL, Finlayson CM (1999) An assessment of the usefulness of remote sensing for wetland inventory and monitoring in Australia. In: Finlayson CM, Spiers AG (eds) Techniques for enhanced wetland inventory and monitoring. Supervising Scientist Report 147, Supervising Scientist, Canberra

Phinn S, Roelfsema C, Decker A, Brando V, Anstee J (2008) Mapping seagrass species, cover and biomass in shallow waters: an assessment of satellite multi-spectral and airborne hyperspectral imaging systems in Moreton Bay (Australia). Remote Sens Environ 112:3413–3425

Pinnel N, Heege T, Zimmermann S (2004) Spectral discrimination of submerged macrophytes in lakes using hyperspectral remote sensing data. SPIE Proc Ocean Opt XVII 1:1–16
Pittenger RF (1989) Exploring and mapping the seafloor. Nat Geosci 177:61A
Pu R, Bell S, Baggett L, Meyer C, Zhao Y (2012) Discrimination of seagrass species and cover classes with in situ hyperspectral data. J Coast Res 28:1330–1334 (in press)
Pulich W Jr, Blair C, White WA (1997) Current status and historical trends of seagrass in the Corpus Christi Bay National Estuary Program study area. Publication CCBNEP-20. Texas Natural Resource Conservation Commission, Austin, p 131
Purkis SJ (2005) A 'reef-up' approach to classifying coral habitats from IKONOS imagery. IEEE Trans Geosci Remote Sens 43:1375–1390
Purkis SJ, Graham NAJ, Riegl BM (2008) Predictability of reef fish diversity and abundance using remote sensing data in Diego Garcia (Chagos Archipelago). Coral Reefs 27:167–178
Purkis S, Klemas V (2011) Remote sensing and global environmental change. Wiley-Blackwell, Oxford
Purkis SJ, Kenter JAM, Oikonomou EK, Robinson IS (2002) High-resolution ground verification, cluster analysis and optical model of reef substrate coverage on Landsat TM imagery (Red Sea, Egypt). Int J Remote Sens 23:1677–1698
Raber GT, Jensen JR, Hodgson ME, Tullis JA, Davis BA, Berglund J (2007) Impact of Lidar nominal post-spacing on DEM accuracy and flood zone delineation. Photogramm Eng Remote Sens 73:793–804
Ramsey E, Rangoonwala A (2005) Leaf optical property changes associated with the occurrence of Spartina alterniflora dieback in coastal Louisiana related to remote sensing mapping. Photogramm Eng Remote Sens 71:299–311
Ramsey E, Rangoonwala A (2010) Mapping the onset and progression of marsh dieback. In: Wang J (ed) Remote sensing of coastal environment. CRC Press, Boca Raton
Rao BRM, Dwivedi RS, Kushwaha SPS, Bhattacharya SN, Anand JB, Dasgupta S (1999) Monitoring the spatial extent of coastal wetlands using ERS-1 SAR data. Int J Remote Sens 20:2509–2517
Rasher ME, Weaver W (1990) Basic photo interpretation: a comprehensive approach to interpretation of vertical aerial photography for natural resource applications. US Department of Agriculture, Washington, DC
Rosenqvist A, Finlayson CM, Lowry J, Taylor D (2007) The potential of long-wavelength satellite-borne radar to support implementation of the Ramsar Wetland Convention. Aquat Conserv Mar Freshw Ecosyst 17:229–244
Rosso PH, Ustin SL, Hastings A (2005) Mapping marshland vegetation of San Francisco Bay, California, using hyperspectral data. Int J Remote Sens 26:5169–5191
Sabol BM, Melton REJR, Chamberlain R, Doering P, Haunert K (2002) Evaluation of a digital echo sounder system for detection of submersed aquatic vegetation. Estuaries 25:133–141
Sallenger AH, Krabill WB, Brock JC, Swift RN, Jansen M, Manizade S, Richmond B, Hampto M, Eslinger D (1999) Airborne laser study quantifies El Niño-induced coastal change. Am Geophys Union EOS Trans 80:89–93
Schmid KA, Hadley BC, Wijekoon N (2011) Vertical accuracy and use of topographic LIDAR data in coastal marshes. J Coast Res 27:116–132
Schmidt KS, Skidmore KA (2003) Spectral discrimination of vegetation types in a coastal wetland. Remote Sens Environ 85:92–108
Schmidt KS, Skidmore AK, Kloosterman EH, Van Oosten H, Kumar L, Janssen JAM (2004) Mapping coastal vegetation using an expert system and hyperspectral imagery. Photogramm Eng Remote Sens 70:703–716
Schweitzer D, Armstrong RA, Posada J (2005) Remote sensing characterization of benthic habitats and submerged vegetation biomass in Los Roques Archipelago National Park, Venezuela. Int J Remote Sens 26:2657–2667
Shalaby A, Tateishi R (2007) Remote sensing and GIS for mapping and monitoring land cover and land-use changes in the Northwestern coastal zone of Egypt. Appl Geogr 27:28–41

Shan J, Hussain E (2010) Object-based data integration and classification for high-resolution coastal mapping. In: Wang J (ed) Remote sensing of coastal environment. CRC Press, Boca Raton

Silva TSF, Costa MPF, Melack JM, Novo EMLM (2008) Remote sensing of aquatic vegetation: theory and applications. Environ Monit Assess 140:131–145

Simard M, Fatoyinbo LE, Pinto N (2010) Mangrove canopy 3D structure and ecosystem productivity using active remote sensing. In: Wang J (ed) Remote sensing of coastal environment. CRC Press, Boca Raton

Sinclair M (2008) Airborne LiDAR hydrographic survey for homeland security. Sea Technol 49:15–20

Stockdon HF, Sallenger AH, List JH, Holman RA (2002) Estimation of shoreline position and change using airborne Lidar topographic data. J Coast Res 18:502–513

Stockdon HF, Doran KS, Sallenger AH (2009) Extraction of LiDAR-based dune-crest elevations for use in examining the vulnerability of beaches to inundation during hurricanes. J Coast Res 35:59–65

Stoker JM, Tyler DJ, Turnipseed DP, Van Wilson K, Oimoen MJ (2009) In: Brock and Purkis (eds) Integrating disparate Lidar datasets for a regional storm tide inundation analysis of Hurricane Katrina. J Coast Res 66–72, Special issue 53, Coastal Applications of Airborne Lidar

Thieler ER, Danforth WW (1994) Historical shoreline mapping: improving techniques and reducing positioning errors. J Coast Res 10:539–548

Thomson AG, Fuller RM, Sparks TH, Yates MG, Eastwood JA (1998) Ground and airborne radiometry over intertidal surfaces: waveband selection for cover classification. Int J Remote Sens 19:1189–1205

Thompson RL, Schroeder AJ Jr (2010) High-definition 3-D tools for underwater surveying and inspection. Sea Technol 51:43

Tiner RW (1996) Wetlands. In: Manual of photographic interpretation, 2nd ed. American Society for Photogrammetry and Remote Sensing, Falls Church, 2440 p

Townsend PA (2000) A quantitative fuzzy approach to assess mapped vegetation classifications for ecological applications. Remote Sens Environ 72:253–267

Townsend PA (2002) Relationships between forest structure and the detection of flood inundation in forested wetlands using C-band SAR. Int J Remote Sens 23:443–460

Townsend P, Walsh S (1998) Modeling floodplain inundation using an integrated GIS with radar and optical remote sensing. Geomorphology 21:295–312

Töyrä J, Pietroniro A, Martz LW (2001) Multisensor hydrologic assessment of a freshwater wetland. Remote Sens Environ 75:162–173

Töyrä J, Pietroniro A, Martz LW, Prowse TD (2002) A multi-sensor approach to wetland flood monitoring. Hydrol Process 16:1569–1581

Valta-Hulkkonen K, Pellika P, Tanskanen H, Ustinov A, Sandman O (2003) Digital false color aerial photographs for discrimination of aquatic macrophyte species. Aquat Bot 75:71–88

Valta-Hulkkonen K, Kanninen A, Pellikka P (2004) Remote sensing and GIS for detecting changes in the aquatic vegetation of a rehabilitated lake. Int J Remote Sens 25:5745–5758

Wabnitz CC, Andrefouet S, Torres-Puliza D, Muller-Karger FE, Kramer PA (2008) Regional-scale seagrass habitat mapping in the Wider Caribbean region using Landsat sensors: applications to conservation and ecology. Remote Sens Environ 112:3455–3467

Wang Y (2010) Remote sensing of coastal environments: an overview. In: Wang J (ed) Remote sensing of coastal environments. CRC Press, Boca Raton

Wang Y, Christiano M, Traber M (2010) Mapping salt marshes in Jamaica Bay and terrestrial vegetation in Fire Island National Seashore using QuickBird satellite data. In: Wang J (ed) Remote sensing of coastal environments. CRC Press, Boca Raton

Wang L, Sousa WP, Gong P (2004) Integration of object-based and pixel-based classification for mapping mangroves with IKONOS imagery. Int J Remote Sens 25:5655–5668

Ward DP, Hamilton SK, Jardine TD, Pettit NE, Tews EK, Olley JM, Bunn SE (2012) Assessing the seasonal dynamics of inundation, turbidity and aquatic vegetation in the Australian wet-dry tropics using optical remote sensing. Ecohydrology. doi:10.1002/eco.1270

Waycott M, Duarte CM, Carruthers TJB, Orth RJ, Dennison WC, Olyarnik S, Calladine A, Fourqurean JW, Heck KL, Hughes AR, Kendrick GA, Kenworthy WJ, Short FT, Williams SL (2009) Accelerating loss of seagrasses across the globe threatens coastal ecosystems. Proc Natl Acad Sci 106:12377–12381

Webster TL, Forbes DL, Dickie S, Shreenan R (2004) Using topographic lidar to map flood risk from storm-surge events for Charlottetown, Prince Edward island, Canada. Can J Remote Sens 30:64–76

West GR, Lillycrop WJ, Pope RW (2001) Utilization of airborne LiDAR bathymetry for rapid environmental assessment. Sea Technol 42:10

Williams DJ, Rybicki NB, Lombana AV, O'brien TM, Gomez RB (2003) Preliminary investigation of submerged aquatic vegetation mapping using hyperspectral remote sensing. Environ Monit Assess 81:383–392

Wilson BA, Rashid H (2005) Monitoring the 1997 flood in the Red River Valley using hydrologic regimes and RADARSAT imagery. Can Geogr 49:100–109

Wolter PT, Johnston CA, Niemi GJ (2005) Mapping submerged aquatic vegetation in the US Great Lakes using Quickbird satellite data. Int J Remote Sens 26:5255–5274

Wozencraft JM, Lillycrop WJ (2003) Airborne coastal mapping, past, present, and future. J Coast Res 38:207–215 (special issue)

Wozencraft JM, Millar D (2005) Airborne lidar and integrated technologies for coastal mapping and charting. Marine Technol Soc J 39:27–35

Yang X (2009) Remote sensing and geospatial technologies for coastal ecosystem assessment and management. Springer-Verlag, Berlin

Yang J, Artigas FJ (2010) Mapping salt marsh vegetation by integrating hyperspectral and LiDAR remote sensing. In: Wang J (ed) Remote sensing of coastal environment. CRC Press, Boca Raton

Yang C, Everitt JH, Fletcher RS, Jensen JR, Mausel PW (2009) Mapping black mangrove along the south Texas gulf coast using AISA+ hyperspectral imagery. Photogramm Eng Remote Sens 75:425–436

Young SS, Wang CY (2001) Land-cover change analysis of China using global-scale Pathfinder AVHRR Landcover (PAL) data, 1982–92. Int J Remote Sens 22:1457–1477

Yuan D, Elvidge CD, Lunetta RS (1998) Survey of multispectral methods for land cover change analysis. In: Lunetta RS, Elvidge CD (eds) Remote sensing change detection: environmental monitoring methods and applications. Ann Arbor Press, Ann Arbor, p 21

Zhang X (2010) On the estimation of biomass of submerged vegetation using Landsat thematic mapper (TM) imagery: a case study of the Honghu Lake, PR China. Int J Remote Sens 19:11–20

Zhou G (2010) Coastal 3D change pattern analysis using LiDAR series data. In: Wang Y (ed) Remote sensing of coastal environments. CRC Press, Boca Raton